Electronic Supplementary Material (ESI) for Energy Advances.

Supplementary Information

Slow Hole Diffusion Limits the Efficiency of *p*-Type Dye-Sensitized Solar Cells Based on the P1 Dye

Maria B. Brands,[a] Olivier C. M. Lugier,[a] Kaijian Zhu,[b] Annemarie Huijser,[b] Stefania Tanase,[a] Joost N. H. Reek*[a]

[a] *van 't Hoff Institute for Molecular Sciences, University of Amsterdam, Science Park 904, 1098 XH, Amsterdam, The Netherlands*

[b] *MESA+ Institute for Nanotechnology, University of Twente, Hallenweg 23, 7522 NH, Enschede, The Netherlands*

Table of Content

1. Preparation of the benchmark P1 *p*-DSSCs

1.1 Cleaning of the FTO glass

In general, to avoid contaminations, the fluorine-doped tin oxide coated glass slides (FTO) was handled with clean gloves only, and only touched on the sides or the non-conductive glass side. The FTO slides were placed on lint-free medical wipes and/or in clean, plastic trays, to avoid fibres and dust particles on the FTO surface. Furthermore, the plates were only put down with the conductive side facing upwards, also to avoid contamination.

The as-received FTO coated glass slides (Sigma Aldrich, 30×30 cm, 2.3 mm thickness, 13 Ω/sq) was cut in nine pieces of 10×10 cm and the conductive side was marked using a glass etching pen. The plates scrubbed with scouring powder and warm water, and scrubbed with Deconex Forte 24 and warm tap water. The conductive side of the FTO was wiped with an acetone-soaked tissue, and rinsed with acetone, toluene and EtOH.

Two plates were placed in a glass prep-TLC developing chamber (which was not used for anything other than cleaning FTO), facing each other with their conductive side in a V-shape. The chamber was filled with Milli-Q ultra-pure water (18.2 MΩ·cm) and a teaspoon of Deconex Forte 24, placed in a holder for the sonication bath and sonicated for 30 min. The solutions were replaced with pure Milli-Q, followed by absolute EtOH, and sonicated for 30 min in both cases. The FTO used for Pt electrodes were additionally sonicated in a dilute HCl solution (0.83 mL concentrated aqueous HCl in 100 mL EtOH) for 30 min. Afterwards, the plates were left to airdry, and stored in clean plastic boxes. Within 24 h after this cleaning procedure, the plates were put in an UV–ozone reactor (UVP PR-100) for a minimum of 30 min, with the conductive side facing upwards. The plates were directly used for one of the following steps afterward.

1.2 NiO blocking layer[1]

After the UV-ozone treatment, the plates were cut up in 50 × 25 mm pieces. Electrodeposition was carried out on a Autolab PGSTAT101 potentiostat (Metrohm) equipped with NOVA software. The FTO was used as working electrode, and it was made sure that the conductive side was facing the Pt mesh (99.99%, 25 × 25 mm, Sigma Aldrich) counter electrode. An alligator clip made electric contact between the potentiostat and FTO, and contact between the clip and the solution was avoided. The Ag/AgCl (3 M KCl) reference electrode (eDAQ, ET069) was placed in between the working and counter electrode, which are depicted in Figure SI–1. The glassware was filled with a $Ni(OAc)_2 \cdot 4H_2O$ solution (0.13 M in Milli-Q).

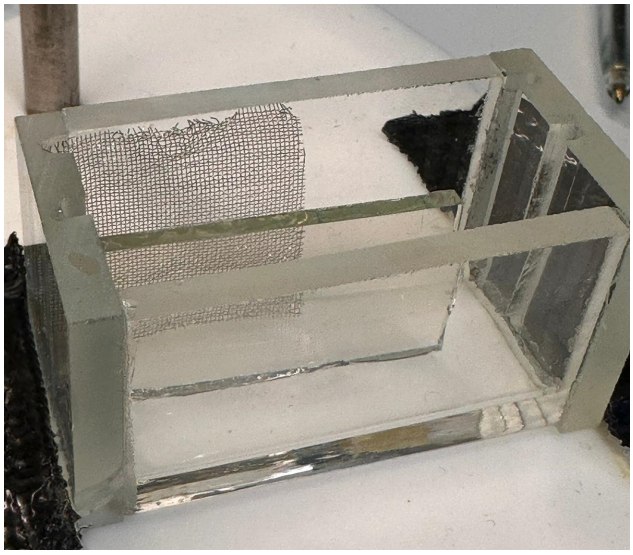

Figure SI–1. A picture of the glassware containing the working electrode (FTO) and counter electrode (Pt mesh) used to create the NiO blocking layer.

The FTO plates were immersed in the $Ni(OAc)_2$ bath, except for a small edge needed for electrical contact, and a potential of 1.1 V (vs. Ag/AgCl) was applied for 120 s. Once the electrodeposition completed, a grey hue was visible on the FTO where it had been in contact with the solution (NiOOH). The plates were rinsed with Milli-Q water and the non-treated edge of the FTO was cut off. The NiOOH films were thermally annealed at 300 °C (with

a temperature ramp of 15 °C·min^{-1}) for 1 h to obtain a thin NiO layer on the FTO. After cooling to room temperature, the plates were stored in a desiccator, in clean, closed, plastic boxes.

1.3 Preparation of NiO | FTO electrodes via doctor-blading

The record-breaking P1-benchmarked NiO electrodes of Suzuki[2] and Sun[3] are based on synthesizing their NiO nanoparticles in-house, by doctor-blading a Ni salt precursor gel onto FTO glass, followed by sintering at 450°C. Below, this route is covered step-by-step, in more detail than has been reported in literature so far. Our procedure is a boiled-down concentrate of many trial-and-error experiments. Although not every experimental decision/pathway is supported by comparative data with the associated error margins, this experimental procedure has, in or our experience, led to the most reproducible and best-performing NiO electrodes. Nevertheless, error margins are still significant, and increasing the reproducibility of this procedure may need further investigation.

Anhydrous $NiCl_2$ was stored under argon in a desiccator. The $NiCl_2$ precursor solution consisted of 1.00 g of anhydrous $NiCl_2$ (Sigma Aldrich, 99.99% trace metals basis), 1.00 g Pluronic F108, 3 g Milli-Q water, and 6 g ethanol (spectroscopic grade). The green solution was heated at 30 °C for at least three days, after which the solution was centrifuged at 4000 rpm for 15 minutes. The green solution was decanted from the remaining solid and stored in a 20 mL vial in a dark safety cabinet.

A strip of Scotch Magic Tape ® was taped on an empty A4 sticker sheet (*i.e.*, without the stickers). Dust was blown off the sheet beforehand with compressed air and care was taken to ensure the tape did not wrinkle or had air bubbles beneath it. Holes were punched in the tape with a circular punch cutter (diameter of 1/4", EK tools, bol.com), while keeping a distance of at least 0.5 cm between the holes. The sheet was cut into pieces, keeping at least 0.25 cm of tape around the holes.

The FTO with electrodeposited NiO was cut into pieces of 1 × 2.5 cm, while keeping the NiO side facing upwards. Care was taken to remove glass splinters and dust particles from the surface, by blowing them off gently with compressed air. A piece of tape was pulled from the sticker sheet and placed on the conductive side of the FTO glass. The best connection between the tape and the FTO was obtained by putting the tape on while touching one side of the slide, and letting it slide/drop slowly in a single movement onto the FTO. The tape should significantly stick over on one side of the slide, which makes it easier to take the tape off later on. The tape was *gently* pressed on the FTO surface, by using either the tip of plastic tweezers or by applying some pressure with a finger on a glass slide.[4] By blowing some compressed air over the bare spot of FTO, any leftover dust particles were removed from the surface.

An ethanol-soaked medical wipe and a clean glass rod were placed within reach. With a glass Pasteur pipette and a small rubber pipette bulb, one drop of the $NiCl_2$ precursor solution was placed in one hole each, and the solution was applied on a maximum of five plates at the same time. The pipette was then emptied back into the $NiCl_2$ precursor solution, and the pipette was placed on another clean glass pipette to avoid contamination of the tip. Within seconds (maximum of one minute) after placing the drops in the holes, the drops were smeared out diagonally using the clean glass rod. The glass rod was firmly held parallel to the FTO surface and moved up and down thrice. Upon the last movement across the plate, the rod was moved to the piece of tape that was sticking over the side, and any excess precursor solution was pushed off the plate that way.[5] We have tried other methods to spread the solution in the well (doctor-blading), but in our experience, this technique gave the most reproducible results.[6]

The glass rod was directly cleaned by wiping with the ethanol-soaked medical wipe, followed by wiping with a dry medical wipe. The procedure is then repeated until all desired FTO-plates have been doctor-bladed. The plates are then left to air dry for at least 30, at most 90 min, before the tape is gently pulled off the FTO surface, using tweezers.[7] This leaves a transparent, circular sol–gel spot. Care is taken to ensure that this sol–gel spot is left undisturbed, which can happen readily when peeling off the tape, or by touching it with the tweezers. Damage to this sol–gel spot will automatically result into a damaged NiO surface, and thus to reproducibility issues.

A large rectangular crucible was placed in the furnace upside down. The FTO plates were placed on top of the crucible. In our experience, the position of the plates in the furnace, as well as the amount of plates in the oven, tend to influence the outcome of the resulting NiO plates.[8] The plates were thermally annealed in a chamber furnace (Carbolite Gero CWF 1100) at 450 °C, with a temperature ramp of 15 °C/min (starting at room temperature), and kept at 450 °C for 30 min. In the meantime, a glass plate on top was heated to 180 °C on a hot plate. Once the

furnace programme had finished, and the NiO spots had a transparent grey colour,[9] the plates were taken out of the furnace immediately transferred to the 180 °C glass plate using stainless steel tweezers.[10]

Once all plates were removed from the furnace, the plates were cooled to 120 °C and left at this temperature. They were either dipped in dye solution directly at this temperature or removed from the heating source and doctor-bladed another time. In the latter case, the procedure reported above was repeated until the desired number of NiO layers was obtained.[11]

In general, the NiO | FTO electrodes look like the example depicted in Figure SI–2: homogeneously light grey and transparent. When twisted sidewards, while letting a light source (such as daylight) diffract on it, a rich colour palette is observed (Figure SI–2, right). Other forms of NiO have also been observed but are hard to reproduce and usually lead to a lower performance (see note 8 and Figure SI–3). The film morphology was investigated by high-resolution scanning electron microscopy (Zeiss MERLIN HR-SEM), as is shown in Figure SI–4, and showed a homogeneous layer of NiO nanoparticles. The multiple layers of NiO could be clearly observed via cross-sectional SEM imaging (Figure SI–5).

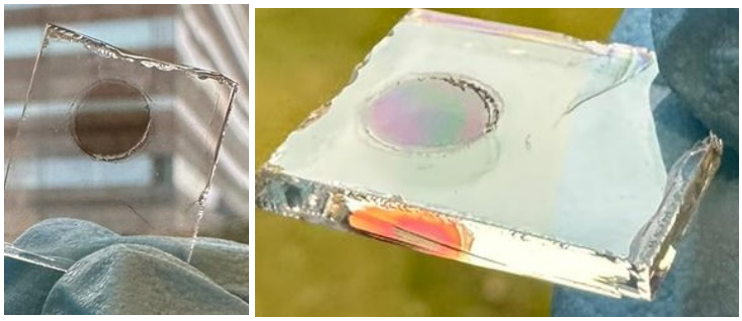

Figure SI–2. General desired visual appearance of the NiO spot on the FTO electrode. Left: top view, right: top view under angle (the diffraction of daylight can be seen on the NiO spot).

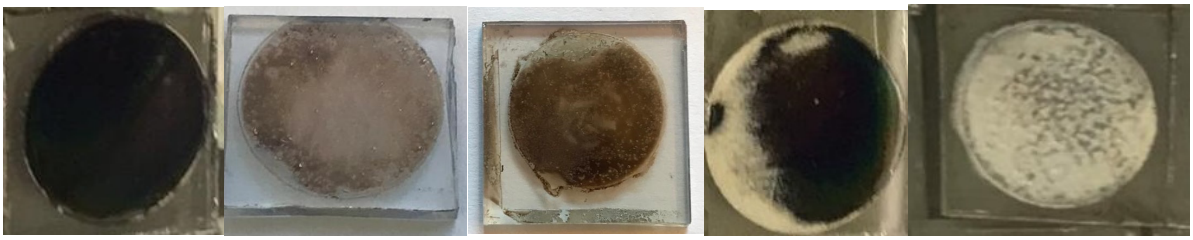

Figure SI–3. Other observed visual appearances of NiO, which have usually led to poor reproducibility and/or lower performance.

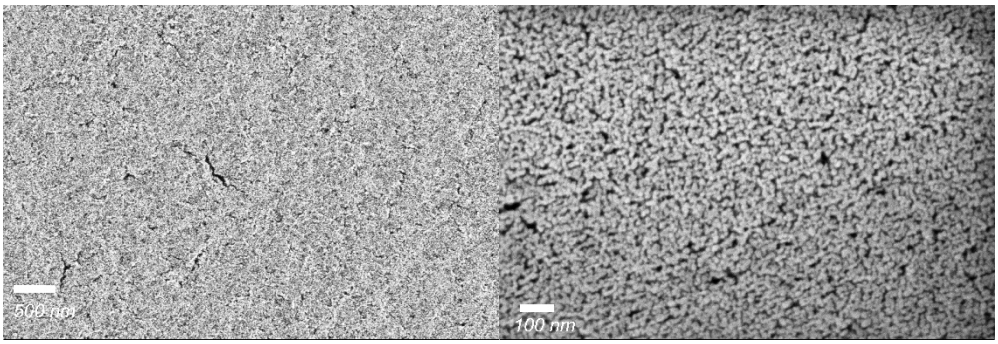

Figure SI–4. Typical SEM image (top view) of the as-prepared NiO layer. In this sample, a single layer of NiO was applied. The left image is less magnified (50 K X) than the right (200 K X). The scales are indicated with the white bar (left: 500 nm, right: 100 nm).

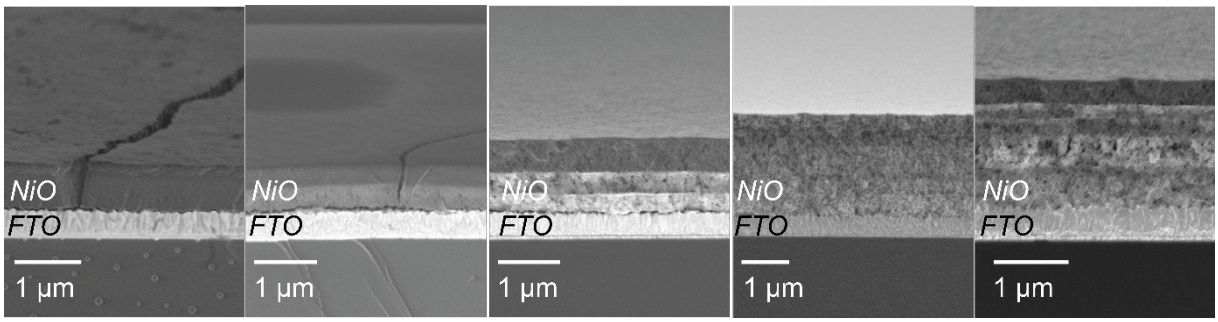

Figure SI–5. Cross-sectional SEM images of an increasing number of NiO layers on FTO (from left to right: one to five layers). The scales (1 µm) are indicated with the white bar.

1.4 Synthesis of the Pt | FTO counter electrodes via electrodeposition

The as-received FTO glass (Sigma Aldrich, 30 × 30 cm, 2.3 mm thickness, 13 Ω/sq) was cut in nine pieces of 10×10 cm. Holes (0.4 mm) were laser-cut into the glass, with a distance of 1.25 cm apart, so that every counter electrode (1.25 × 2.5 cm) contains one hole. The plates were cleaned according to the procedure described in '*Cleaning of FTO glass*'.

Pt was electrodeposited on the FTO according to Lin et al. and Reek et al.,[12,13] where FTO was used as working electrode, Ag/AgCl (in 3 M KCl) as reference electrode (eDAQ, ET069) and Pt mesh (99.99%, 25 × 25 mm, Sigma Aldrich) as counter electrode. The electrodes were immersed in a solution of $PtCl_4$ (10 mM), 3-(2-aminoethylamino)propyl-methyldimethoxysilane (0.47 mM) and HCl (50 mM) in milli-Q, and a current of 25 mA was applied for 30 s (setup depicted in Figure SI–1). The electrodes turned dark metallic grey after electrodeposition and were rinsed with absolute ethanol and airdried. They were stored in a closed plastic box at ambient conditions.

1.5 Dye-sensitization of the NiO electrodes

The doctor-bladed NiO electrodes at 120 °C were inserted into in a room temperature solution of P1 (Dyenamo) in dry acetonitrile (0.3 mM, Acros) and kept in solution (in the dark) for at least 16 hours. After removal from the solution, the plates were rinsed with excess MeCN and airdried. Once dry, the plates were stored in a plastic container, covered by aluminium foil, in a desiccator. The resulting electrodes are displayed in Table SI–1.

Table SI–1. Overview of the visual appearance of the P1-sensitized NiO electrodes before assembly into the DSSC.

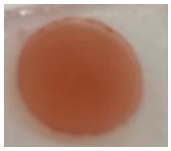 1a	 1b	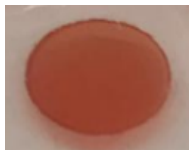 1c	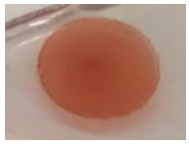 1d
 2a	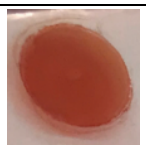 2b	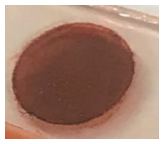 2c	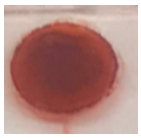 2d
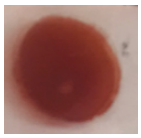 3a	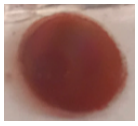 3b	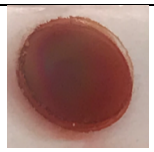 3c	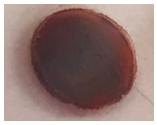 3d
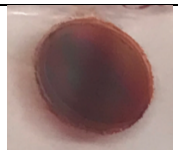 4a	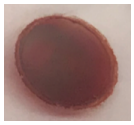 4b	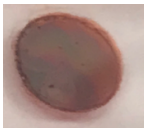 4c	 4d
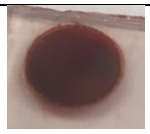 5a	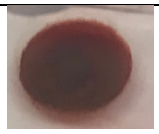 5b	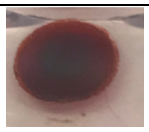 5c	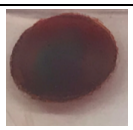 5d

1.6 Sandwich cell assembly[14]

Since the DSSCs are assembled by hand, there can be some deviations between different solar cells. In some cases, the cause for the deviating behaviour was very clear (e.g. a large air bubble inside the DSSC, or a broken FTO electrode).

The dyed electrodes were assembled face-to-face to the platinum counter electrode, using a 60 µm thick thermoplastic frame (Surlyn®, Meltonix 1170-0, Solaronix, Switzerland). A ¼" diameter hole was punched in the thermoplastic frame, which is the same size as the NiO spot, using a circular punch (EK tools, bol.com). A sharp edge of the hole[15] was realized by putting the plastic in between to regular paper sheets. The thermoplastic frame was then melted by rolling a soldering iron (at 350 °C) over the cell on the side of the Pt counter electrode (rolling over this side avoids dye decomposition).

The electrolyte solution, consisting of 0.1 M I_2 and 1.0 M LiI (Sigma Aldrich, Anhydrobeads™, 99.999% trace metal basis) in dry MeCN, should be prepared on the day of the solar cell assembly and measurements. Dry MeCN is used straight from the bottle but filtered over a syringe filter. LiI is sensitive to light and thus should be weighed in the dark and stored under argon in the dark at 4 °C. Light-induced decomposition of LiI is indicated by a color change from white to deep red-brown. Furthermore, during the assembly, the solution should be kept in the dark, by covering the vial with aluminum foil or by using a brown vial.

Once the two electrodes were melted together, the ends of the electrodes were painted with conductive silver paint (Ted Pella, Inc.) which was left to dry for 30 min. Subsequently, the electrolyte was introduced via the hole by the vacuum-backfilling method. During this method, the hole is covered with a drop of electrolyte. The cell is then placed in a chamber under reduced pressure, which causes the air inside the cell to evacuate, and the electrolyte to enter the cell. Once the air has escaped the cell, indicated by air bubbles going through the electrolyte drop and the absence of air bubbles inside the hole, the reduced pressure should be released as soon as possible. Applying

reduced pressure for longer times can lead to evaporation of MeCN and consequent alteration of the LiI/I_2 concentrations.[16] The hole was then sealed by putting a piece of thermoplastic on a glass slide, melting it with the soldering iron, and pressing it with the thermoplastic side down on the hole. Proper attachment was achieved by pressing the cover slide down with the soldering iron and ensuring that all the thermoplastic melted to the back side of the Pt electrode. This prevents electrolyte from evaporating over time/under illumination.

Finally, a reflective layer of aluminium foil was attached to the back of the cell. A piece of thermoplastic was put right above the NiO spot, on top of which a piece of aluminium foil was placed. The whole was melted together under a heat press at 120 °C, by gently pressing on the cell for two seconds. A mask, consisting of two layers of black tape (PVC tape, Conrad) with a 3/16" diameter hole punched in it (punching was carried out similarly as in the NiO doctor blading section above to create a sharp edge). A full overview of the DSSC assembly can be found in Figure SI–6. The solar cells were directly measured after assembly.

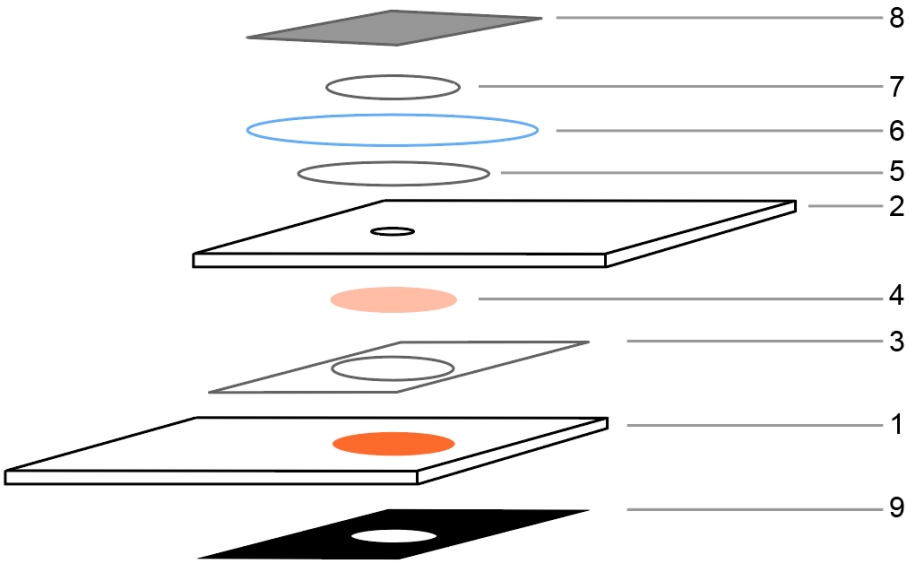

Figure SI–6. An overview of the sandwich cell: 1 = P1 | NiO | FTO electrode; 2 = Pt | FTO counter electrode with ø 60 µm hole; 3 = 60 µm thick thermoplastic frame with ø¼" hole; 4 = electrolyte (1 M I^-/I_3^- in dry MeCN); 5 = 60 µm thick thermoplastic polymer to seal electrolyte hole; 6 = cover slide; 7 = 60 µm thick thermoplastic polymer to attach piece of aluminium foil; 8 = piece of aluminium foil (shiny side facing inside cell); 9 = the mask, *i.e.*, a piece of black tape with ø 3/16" (or 0.17814 cm^2) hole.

2. Characterization of the P1 | NiO | FTO electrodes

2.1 NiO thickness

We measured the thickness of the P1 | NiO | FTO electrodes **after** completion the photoelectrochemical measurements, since a small scratch needed to be made into the NiO to accurately determine the thickness, which could influence the photoelectrochemical results. After completing the measurements, the solar cells were disassembled, by placing them under the heat press (Zonesun ZS–90, AliExpress) at 200 °C, with the NiO side of the cell facing upwards, in contact with the hot press. After 10 seconds, the cell could be pulled apart by hand (while wearing oven gloves). There will remain some residue of the Surlyn polymer on the FTO of the NiO electrode, and the P1 dye on the surface was decomposed after this step, as the red colour had disappeared.

The thickness of the NiO plates was characterized with a mechanical profilometer (P7, KLA-Tencor) with a stylus of radius 2 µm with a 60° cone angle, applied load of 1 mg and a scan speed of 20 $\mu m \cdot s^{-1}$. A small scratch was applied in the NiO film with a *dull* needle, as shown in Figure SI–7, after which a cross-sectional profile was measured through this scratch, in the centre of the NiO spot. We confirmed that the FTO/glass layer was not scratched during this process. The results of the individual NiO electrodes are given in Table SI–2.

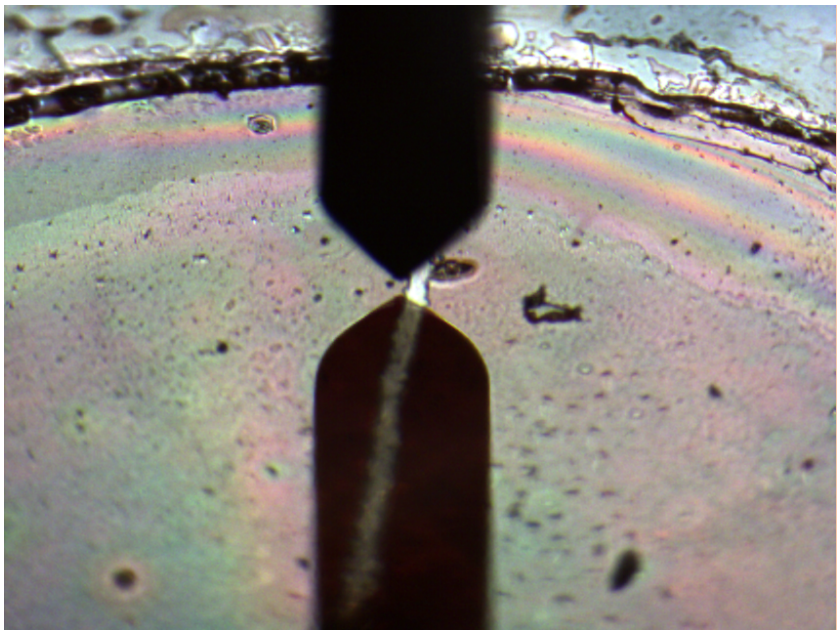

Figure SI–7. Depiction of the scratch in the NiO film and the position of the profilometer tip.

Table SI–2. The thickness of the NiO layers of the individual electrodes on the FTO substrate.

	NiO thickness (µm)			
NiO layers	a	b	c	d
1	0.57	0.70	0.59	0.66
2	0.87	0.68	1.23	0.96
3	0.93	1.20	1.30	1.75
4	1.85	1.83	1.43	1.19
5	2.04	2.29	2.03	2.26

The mean values in the main text (Table 1) were calculated by averaging the values in Table SI–2. The error analysis was carried out by calculating the root-mean square between the sample mean and the observed values, *i.e.*, the sample standard deviation, using the *stddev* function in Origin (version 2018).

2.2 Dye loading

Dye leaching approaches usually involve strong acids or bases, but P1 shows limited stability under such circumstances. Therefore, dye loading of the P1 | NiO electrodes was quantified by dye desorption under mild conditions, using a phenyl-phosphonic acid solution (1 M in MeOH).[17,18] This strategy is based on the competitive adsorption of an adsorbent which has a stronger affinity to the NiO surface than the carboxylic acid, namely the phosphonic acid group. P1 shows good stability under these circumstances, and the absorption spectrum of P1 in this leaching solution is displayed in Figure SI–8. The absorption maxima of P1 at 349 and 479 nm correspond to extinction coefficients of 22 860 and 44 048 M^{-1} cm^{-1}, respectively. The spectrum in 1 M PPA in MeOH differs from those earlier reported in MeCN,[19] likely due to the different solvent environments.

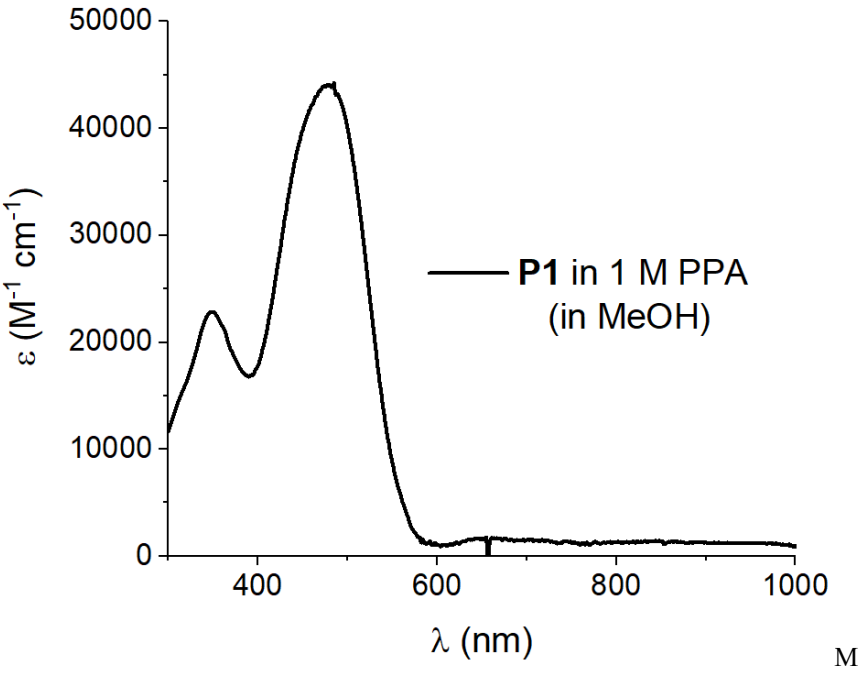

M

Figure SI–8. UV-vis absorption spectrum of **P1** (24.2 μM) in 1 M PPA in MeOH.

Furthermore, phenyl-phosphonic acid itself is a colourless compound, and does therefore not interfere with the absorption of the dye in the visible region. The dye loading was determined by immersing a NiO plate with a surface area of 0.318 cm^2 (r = 1/8" or 0.318 cm) in a 3 mL solution of PPA (1 M in MeOH) for 24 h in a closed vial. The UV-vis absorption of the resulting solution was then measured in a 1 cm cuvette in a UV-vis spectrometer (Hewlett Packard 8453, single beam), and the original dye loading on the NiO plate was calculated with Equation SI–1. For each NiO plate, the dye loading was determined for both absorption maxima (λ = 349 and 479 nm), and the average of the two values was taken.

$$dye\ loading\ (mol \cdot cm^{-2}) = \frac{A(\lambda)}{\varepsilon(\lambda)} \cdot \frac{3 \cdot 10^{-3}}{0.317} \qquad (SI-1)$$

where A(λ) is the absorption at the absorption maxima, ε(λ) is the extinction coefficient according to the data in Figure SI–8, $3 \cdot 10^{-3}$ is the volume of the solution and 0.318 is the surface area of the NiO film in cm^2. The measurement was carried out in triplo for each datapoint. Since the dye loading on NiO cannot be carried out before the photoelectrochemical measurements (due to the strong binding of phenylphosphonic acid), nor after (due to P1 decomposition during DSSC disassembly, see section 'NiO thickness'), these measurements were carried out in different electrodes than those used in the solar cells. Since these electrodes were made in the same batch as those used in the DSSCs, we are convinced the values below are representative of those in the DSSCs. The results are given in Table SI–3, and the mean values were calculated by averaging the values of the individual electrodes. The error analysis was carried out by calculating the root-mean square between the sample mean and the observed values, i.e., the sample standard deviation, using the *stddev* function in Origin (version 2018).

Table SI–3. Dye loading for the different NiO electrode preparations.

	Loading (nmol·cm^{-2})
1	75.31 ± 20.11
2	74.91 ± 12.31
3	111.28 ± 34.19
4	143.37 ± 25.74
5	130.39 ± 15.74

These values were in well within range of earlier reported dye loadings (see Table SI–4). The dye loading on our electrodes is comparable to previously reported doctor-bladed NiO electrodes and is slightly lower than on screen-printed electrodes. It has been noted before that the surface area of NiO prepared by sol–gel methods are often lower than that of those with pre-formed NiO nanoparticles.[20]

Table SI–4. Reported dye loadings of P1 on NiO | FTO electrodes.

Method	Loading (nmol·cm^{-2})	reference
Screen-printing (Reek et al.)	310	14
Doctor-blading	32	21
Doctor-blading	0.003	22
Spray-deposition (Dini et al.)	33	1
Screen-printing (Dini et al.)	200	23
Doctor-blading (Lin et al.)	158	24

The wavelength-dependent light harvesting efficiency, η_{LH}, can also be calculated via Equation 2 (main text), and is plotted in Figure SI–9.

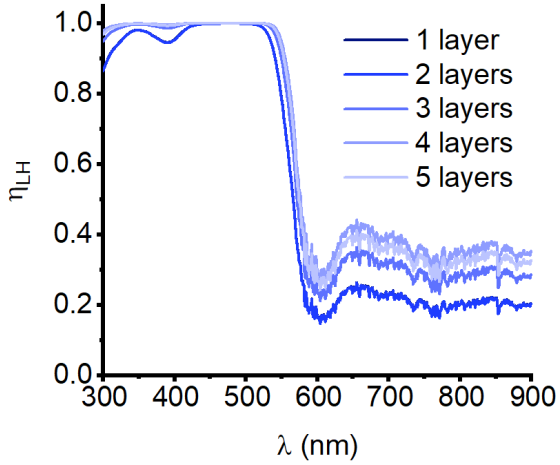

Figure SI–9. Light harvesting efficiencies η_{LH} (λ) derived from the dye loadings above, according to Equation 2 (main text).

To obtain information about the (relative) cumulative light harvesting of the different samples, the light harvesting spectra were integrated using 'integration tool' of the Origin 2018 software, where the limits were fitted to interpolate to rectangle edges, and the area type was set to the mathematical area (see Figure SI–10 for an example). The spectra were integrated from 300–900 nm. The results of the integration can be found in Table SI–5.

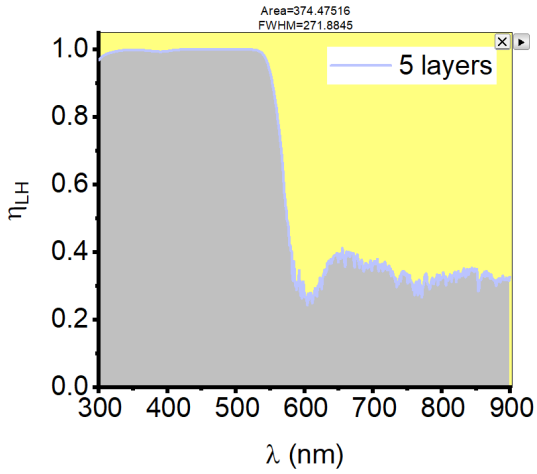

Figure SI–10. Example of an integration of the light harvesting spectrum using the Origin 2018 software package.

Table SI–5. Integrals of the light harvesting efficiency spectra with varying NiO thickness.

Number of NiO layers	Integral light harvesting efficiency
1	323
2	323
3	359
4	384
5	375

3. Solar cell characterization

The assembly of the solar cells by hand is a process that is prone to error. During the assembly of the solar cells, we have noticed that some deviations can arise that heavily influence the outcome of the photoelectrochemical measurements. Therefore, a selection process was carried out. This selection was based on whether the equivalent circuit model for DSSCs, as described in the section Photoelectrochemical Impedance Spectroscopy (PEIS), could be fit to the solar cell data. If this was not the case, these data were excluded from the calculation of averages and the associated error margins. Nonetheless, the individual results are reported here, in the SI. **On average, approximately ~70% of the solar cell assembly was successful, based on the PEIS data.**

In most cases, possible reasons for the deviating behaviour seemed obvious. For instance, an air bubble can be present in the electrolyte, which we were not always able to cover with the mask. This resulted in a lower performance of the solar cell, and additional resistive behaviour. Furthermore, we have noticed that when the vacuum backfilling of the solar cell was not successful in one attempt but had to be repeated, the photoelectrochemical results were influenced as well. One can imagine that applying a vacuum for an extended time could influence the electrolyte concentration due to MeCN evaporation. Finally, in one case (solar cell 4c), the NiO | FTO electrode cracked during assembly. However, there were also cases where above situations did not apply, and deviating behaviour was still observed. For those solar cells, we can only speculate on possible causes, which might include a poor connection between the NiO and FTO, or incomplete sintering due to temperature deviations in the oven.

For all measurements below, a high-power white LED source (T04 in combination with LSW-2, Zahner) was used with an illumination intensity of 100 $mW \cdot cm^{-2}$, and the spectral output of the lamp is shown in Figure SI–11. The illumination intensity was tuned using a photodiode sensor located next to the solar cell (S01, Zahner Elektrik), calibrated to the light source via calibration files obtained from the supplier. The light source and cell were mounted on a rail and placed inside a light exclusion box (Zahner).

For cross-comparison with other work, a 1 sun AM 1.5G reference solar simulator is commonly used. The spectral width of this reference light source is wider than the white LED used here. Therefore, direct comparison of the reported solar cell efficiency (from J–V curves) should proceed with caution. We have not used a solar simulator here, as this study focuses on relating the power conversion efficiency directly the charge dynamics using intensity-modulated light spectroscopy. These latter measurements require specific setups that do not come with our solar simulator that we have used. For the sake of consistency, we thus decided to use the same light source for both sets of measurements. During the measurements, the surface of the solar cells heated up slightly, with a maximum of 7 °C. We did not observe an increased solar cell performance after extended illumination.

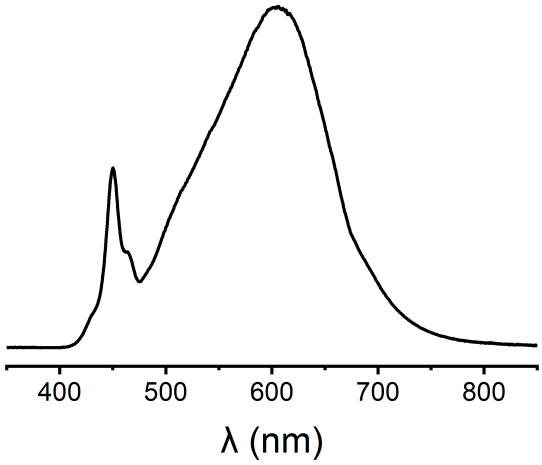

Figure SI–11. Emission spectrum of the high-power white LED source (Zahner T04/LSW-2).

3.1 J–V curve measurements

Current–voltage data was collected with a photoelectrochemical workstation (Zahner Zennium & PP211, Germany). The scan speed was set at 5 $mV \cdot s^{-1}$, starting at V_{OC}, sweeping to J_{SC}, and back to V_{OC}. Two sequential J–V curves were measured, the first one being recorded right after sealing of the solar cell, and the second directly after the first measurement. We observed a slight hysteresis in the first scan, which became negligible in the second scan (see Figure SI–12). Furthermore, the first measurement usually shows higher efficiencies compared to subsequent ones. This could be related to trap states that are not filled yet in the first measurement but do fill after some photocurrent has flown through the system. In our view, the second J–V curve is thus a more representative measurement of the solar cell. The averaged results of the measured J–V curves are shown in Table SI–6. The results for each individual solar cell are shown in Table SI–7. The averaged values in Table SI–6 were determined by calculating the mean of the values in Table SI–7. The error analysis was carried out by calculating the root-mean square between the sample mean and the observed values, *i.e.*, the sample standard deviation, using the *stddev* function in Origin (version 2018).

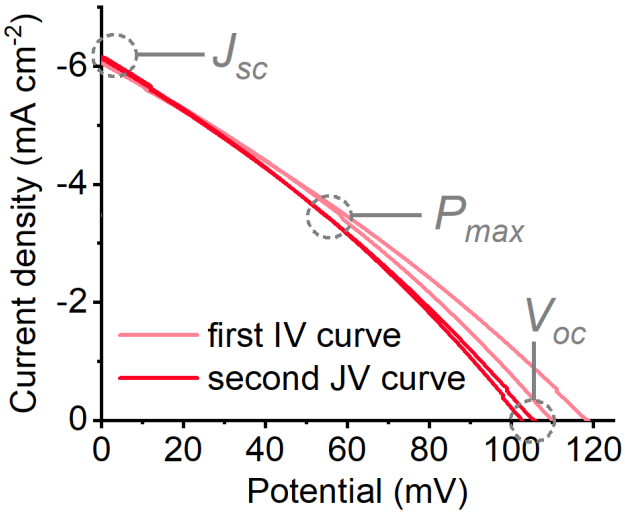

Figure SI–12. Difference between first and second J–V curve (for solar cell 4b).

From the J–V curve, the fill factor and power conversion efficiency (η) could be calculated via the J_{SC}, V_{OC} and P_{max} (which were derived as indicated in Figure SI–11), according to the following equations (Equations SI–2 and SI–3):

$$\eta\ (\%) = \frac{P_{max}}{P_{in}} \qquad (SI-2)$$

$$FF = \frac{P_{max}}{V_{OC}J_{SC}} \qquad (SI-3)$$

where P_{max} is the point of the J–V curve with the highest power output.

Table SI–6. Averaged data for the solar cells, derived from Table SI–7.

Number of NiO layers	V_{oc} (mV)	J_{sc} (mA·cm^{-2})	FF	η (%)
1	106 ± 9	–2.19 ± 0.82	0.318 ± 0.010	0.075 ± 0.029
2	119 ± 20	–2.59 ± 0.95	0.316 ± 0.037	0.093 ± 0.020
3	101 ± 7	–2.94 ± 1.36	0.288 ± 0.028	0.087 ± 0.046
4	107 ± 1	–4.49 ± 1.45	0.277 ± 0.017	0.134 ± 0.049
5	105 ± 2	–4.15 ± 0.81	0.278 ± 0.013	0.121 ± 0.031

Table SI–7. Data derived from J–V curve under 100 mW·cm^{-2} illumination for the individual solar cells. The solar cells that are left out of the study are highlighted in grey, due to deviating behaviour, as became clear from the photoelectrochemical impedance results (as explained at the beginning of this section).

solar cell	η	V_{OC}	J_{SC}	FF
1a	0.088	113	–2.413	0.323
1b	0.032	94	–1.019	0.328
1c	0.096	107	–2.948	0.307
1d	0.083	111	–2.385	0.313
2a	0.089	101	–3.077	0.287
2b	0.114	117	–3.196	0.303
2c	0.006	109	–0.160	0.362
2d	0.075	140	–1.489	0.358
3a	0.041	103	–1.533	0.258
3b	0.087	93	–3.037	0.312
3c	0.133	106	–4.254	0.295
3d	0.009	107	–0.227	0.362
4a	0.098	107	–3.535	0.258
4b	0.19	107	–6.154	0.289
4c	0.011	96	–0.457	0.253
4d	0.106	93	–3.742	0.304
5a	0.143	106	–4.724	0.287
5b	0.099	103	–3.573	0.269
5c	0.014	112	–0.531	0.236
5d	0.072	103	–2.918	0.240

Furthermore, we investigated correlations between the efficiency and the J_{SC}, V_{OC} and fill factor, as depicted in Figure SI–13.The data of J_{SC} vs. η was fitted to a linear function using Origin software (version 2018).

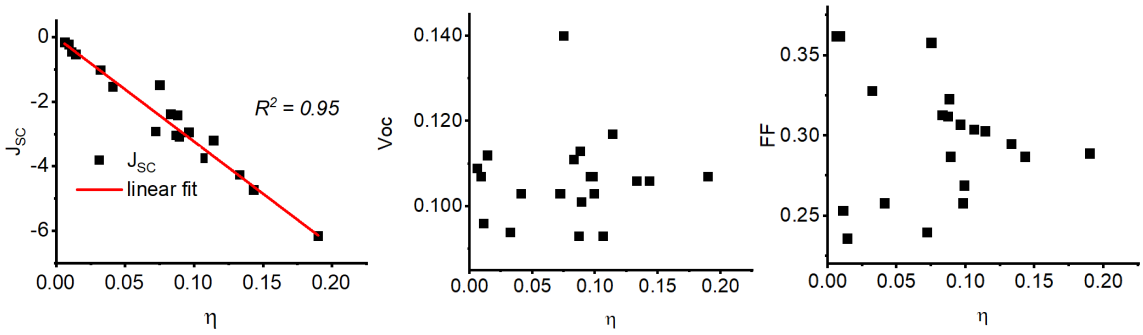

Figure SI–13. Correlation between the solar cell efficiency and J_{SC} (left) V_{OC} (middle) and fill factor (right).

3.2 Determination of hole lifetime (τ_n) with PEIS and IMVS

The hole lifetimes (τ_n) in the dye-sensitized photocathodes were determined via two different methods. Intensity modulated photovoltage spectroscopy (IMVS) is a galvanostatic technique commonly used to determine the hole lifetime at the open circuit potential (J = 0 A).[25] From these measurements, τ_n can be directly derived from the empirical data, which avoids modelling inaccuracies.[26] However, since it is a galvanostatic method, IMVS is rarely used to study the charge dynamics at short circuit conditions (0 V), which are the conditions we are interested in in this work.

To probe this point of the J–V curve, photoelectrochemical impedance spectroscopy (PEIS) is commonly used, as this is a potentiostatic measurement. However, interpretation of the PEIS data requires fitting of the data to an equivalent circuit model (ECM), whereas in IMVS, the hole lifetime can be extracted from the data directly. To confirm the validity of the PEIS model, we carried out both PEIS and IMVS measurements at V_{OC}, and cross-compared their results. They were in excellent agreement (Table SI–8), which indicates that the model used in PEIS accurately describes the DSSC, and can thus be used to determine the hole lifetime at J_{SC}.[25] Subsequently,

the ECM was used to determine τ_n at short-circuit conditions, to accurately determine η_{CC} at this point (Equation 3), which requires τ_c and τ_n to be measured at the same conditions (i.e., at 0 V, illuminated with an intensity of 100 mW·cm^{-2}). [25,27–29] The hole collection times (τ_c) were measured with IMVS and are discussed below in Section 3.3.

In Table SI–8, a complete overview of the obtained lifetimes in the PEIS and IMVS measurements is shown. In the sections below, a detailed description is given of how these values were obtained. Some solar cells were excluded from the hole lifetime analysis, as they could not be analysed accurately, as is explained in detail above (at the beginning of Section 3).

Table SI–8. Individual solar cell data and their corresponding hole lifetime as determined with IMVS (at V_{OC}) and PEIS (at V_{OC} and J_{SC}), in all cases under 100 mW·cm^{-2} intensity illumination (white LED).

Solar cell	τ_n (s)			Solar cell	τ_n (s)		
	IMVS V_{OC}	PEIS V_{OC}	PEIS J_{SC}		IMVS V_{OC}	PEIS V_{OC}	PEIS J_{SC}
1a	0.028	0.024	0.084	3b	0.060	0.060	0.129
1b	0.014	0.011	0.115	3c	0.041	0.037	0.106
1c	0.041	0.029	0.096	4a	0.028	0.026	0.065
1d	0.041	0.030	0.110	4b	0.028	0.024	0.085
2a	0.060	0.054	0.135	4d	0.041	0.042	0.131
2b	0.041	0.039	0.095	5a	0.028	0.027	0.083
2d	0.020	0.017	0.063	5b	0.041	0.062	0.093
3a	0.089	0.074	0.229				

3.2.1 Intensity Modulated Photovoltage Spectroscopy (IMVS)

The controlled intensity modulated photovoltage spectroscopy (CIMVS) measurements were carried out using a Zahner CIMPS photoelectrochemical workstation (Zahner-Elektrik) controlled by CIMPS and Thales Z software packages (Zahner-Elektrik). The photocathodes were backlit with a white LED source (Zahner-Elektrik, TL04/LSW-2, see Figure SI–11 for spectral output). The measurements were carried out in a light exclusion box (Zahner-Elektrik). The cell was measured under galvanostatic conditions, with an applied current of 0 A (open circuit). A dc light intensity of 100 mW·cm^{-2} was applied with an ac perturbation of 10 mW·cm^{-2}. The frequencies were scanned from 100 Hz → 300 mHz, with 10 measuring steps (frequencies)·dec^{-1} above 66 Hz, and 5 steps·dec^{-1} below 66 Hz. At frequencies < 66 Hz, 4 measurement points were averaged at each measurement frequency; at the higher frequencies, 20 points were averaged at each frequency. For every NiO layer, the measurements were carried out at least in duplicate.

The obtained data was imported in the Zahner Analysis software, and the hole lifetime was calculated directly from the complex plane representation (*i.e., Nyquist plot*) of the IMVS response via Equation SI–4:[30–32]

$$\tau_n = \frac{1}{\omega_{min,IMVS}} = \frac{1}{2\pi f_{min,IMVS}} \qquad (SI-4)$$

where $f_{min,IMVS}$ is the frequency corresponding to the minimum of the semicircle, as shown in Figure SI–14.

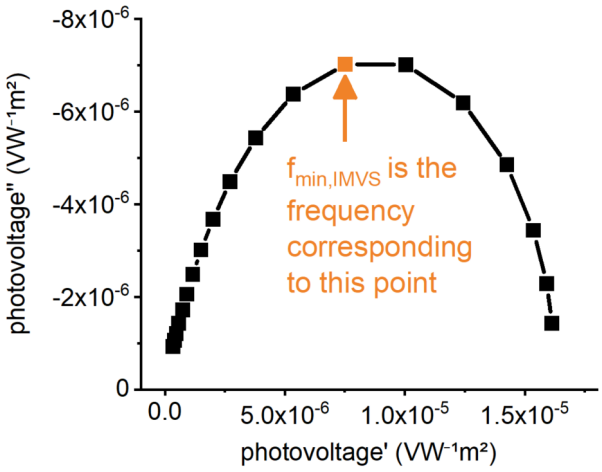

Figure SI–14. How $f_{min,IMVS}$ was derived from the –Nyquist plot of the IMVS data.

In this approach, some assumptions are made when deriving the hole lifetime. The model cannot account of nonlinearities in the photovoltage with respect to light intensity or rate constants that depend on light intensity. It is thus assumed, in this case, that the photovoltage varies linearly with the fluctuating light source. Furthermore, there is a possibility that the measured point did not hit the *actual* maximum.[27] In this case, the determined $f_{min,IMVS}$ deviates. Measuring more steps·dec^{-1} can decrease this deviation, but drastically increases measurement times. Furthermore, the absolute values for the derived rate constants might vary for different measurement setups and should be compared with caution.[27]

3.2.2 Photoelectrochemical Impedance Spectroscopy (PEIS)

The photoelectrochemical impedance (PEIS) measurements were carried out using a Zahner-CIMPS photoelectrochemical workstation (Zahner-Elektrik) controlled by CIMPS and Thales Z software packages (Zahner-Elektrik). The DSSCs were probed through the back of the photocathode side with a white LED source (Zahner-Elektrik, TL04/LSW-2, see Figure SI–11 for spectral output) at a light intensity of 100 mW·cm^{-2}. The irradiation area of the DSSCs with a mask was 0.178 cm^2. The measurements were carried out in a light exclusion box (Zahner-Elektrik). For each solar cell, photoelectrochemical impedance spectroscopy was carried out at dc potentials corresponding to the open circuit potential (V_{oc}) and the short circuit potential (0 V) with an ac perturbation of 5 mV. The frequencies were scanned from 10^{-1} to 10^5 Hz, with 10 measuring steps·dec^{-1} above 66 Hz, and 5 steps·dec^{-1} below 66 Hz. At frequencies < 66 Hz, 4 measurement points were averaged at each measurement frequency; at higher frequencies, 20 points were averaged at each frequency.

PEIS domain data need to be fitted to a model before relevant parameters, such as lifetimes, can be extracted.[27,31] This model consists of an electrical circuit, containing elements that represent the electrochemical processes occurring in the cell, also known as the *Equivalent Circuit Model* (ECM). For *p*-type DSSCs, multiple ECMs have been used to disentangle PEIS data, such as the transmission line model, or the model reported by Wu et al.[31] We have adapted the latter in this work (Figure SI–15). Commonly, two RC–circuits (R = resistor, C = capacitor) are placed in series with each other and with a separate resistor. The separate resistance R_s represents the ohmic resistance of the cell (*e.g.*, the solution and the connections), whereas the RC circuits models the electrochemical processes occurring at the NiO and Pt electrode, respectively. An RC circuit traditionally consists of a resistor and a capacitor. The resistor then models the hindrance of charge transport in the material and across the interface, and the capacitive circuit element models the accumulation of charge in the electrode.[33] However, to account for the frequency dispersion that is usually present in the EIS data, the capacitor is exchanged for a constant phase element, as is the case in the model we are using in this study (Figure SI–15).[33]

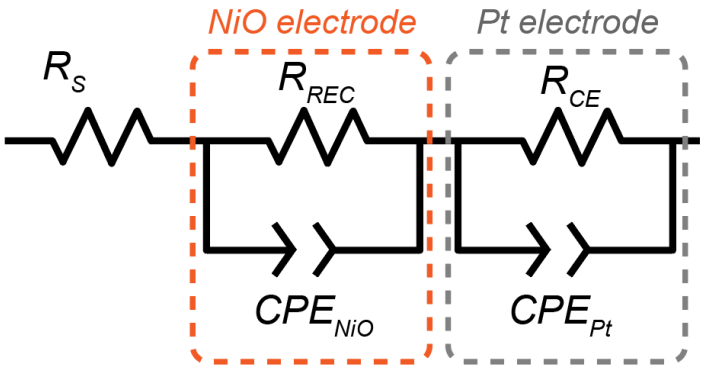

Figure SI–15. The equivalent circuit model (ECM) used in this PEIS study to represent the interfaces in the P1 *p*-DSSC. The R_s element represents the ohmic resistances within the cell (*e.g.*, the solution and connections), whereas the two resistor–constant phase element circuits in series represent the two electrodes (the NiO electrode in the orange box and the Pt electrode in the grey).

The PEIS response both at open circuit and short circuit conditions typically resulted in a Bode plot that shows two peaks in the phase vs. log ω plot (See Figure SI–16, left). The first event occured at high frequency (~1–10 kHz), and was independent of the applied potential and or light intensity. Therefore, this process likely corresponds to the electrochemical processes on the CE. The absolute impedance values around this event were low (>50 Ω) The second event occurs at lower frequency (1–100 Hz), is dependent on the light intensity and applied potential, and is thus likely associated with the processes occurring on the WE. The corresponding Nyquist plot showed two semicircles, each semicircle representing a separate diffusion process (Figure SI–16, right).

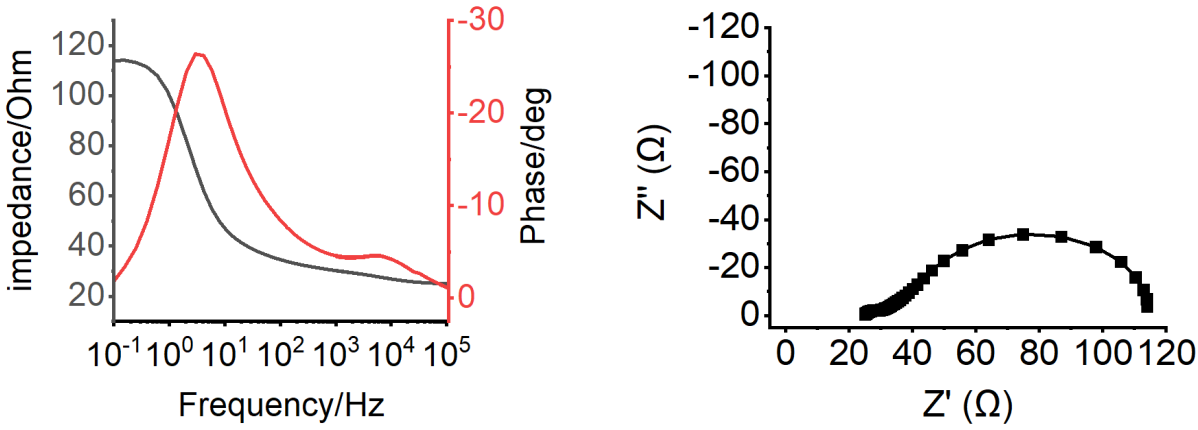

Figure SI–16. The Bode plot (left) and –Nyquist plot (right) of a typical benchmark solar cell. The results here were for solar cell 4b, measured under short circuit conditions, illuminated with 100 mW·cm^{-2} intensity light.

The PEIS results were fitted to the ECM in Figure SI–15 using the Zahner Analysis software (version 3.2.2). The data of the different solar cells did not fit this ECM in all cases. Some solar cells showed additional impedance features, very high overall impedance values (> 1000 Ω), or no varying response over the frequency range. In these cases, the fit to the ECM in Figure SI–15 gave relatively large error values and were excluded from further analyses. Specifically, these considered solar cells *2c*, *3d*, *4c*, *5c* and *5d*.

Values corresponding to the circuit elements are obtained when the data is fitted to the circuit model. For all individual solar cells, these values can be found in Table SI–9. These values were directly used to determine the hole lifetime τ_h (Equation SI–5):[26]

$$\tau_n = R_{rec}C_{\mu} \qquad (SI-5)$$

where R_{rec} (in Ω) is the value directly obtained from the fitting (see Figure SI–15/Table SI–9), and C_{μ} was determined via Equation SI–6:

$$C_{\mu} = \frac{(Y_{rec}R_{rec})^{1/\alpha}}{R_{rec}} \qquad (SI-6)$$

where Y_{rec} is a constant with the dimension of Siemens·sec$^{\alpha}$ or Ss$^{\alpha}$, and α is an empirical constant. These two values were also directly obtained from the fitting (see Table SI–9). The values for τ_n for each solar cell are shown in Table SI–8.

The mean values of τ_n in the main text (Figure 3, right panel) were calculated by averaging the values in Table SI–8. The error analysis was carried out by calculating the root-mean square between the sample mean and the observed values, *i.e.*, the sample standard deviation, using the *stddev* function in Origin (version 2018). The experimental error bars represent one standard deviation.

Table SI–9. Detailed PEIS parameters for the individual DSSCs obtained after fitting the PEIS data to the ECM in Figure SI–15, using the Zahner Analysis software. Due to the strongly deviating behavior of solar cell 5c, the measurements were discarded.

Solar cell	overall error	R_s (Ω)	Error (%)	Sig	R_{REC} (Ω)	Error (%)	Sig	Y_{REC} (Ss^a)	Error (%)	Sig	a_{REC}	Error (%)	Sig	R_{CE} (Ω)	Error (%)	Sig	Y_{CE} (Ss^a)	Error (%)	Sig	a_{CE}	Error (%)	Sig
1a - s	1.59	35.1	1.44	0.988	389	6.88	0.805	2.56E-4	2.79	0.589	0.933	0.49	3.195	41.2	2.75	0.341	3.39E-4	4	0.226	0.552	3.89	0.236
1a - o	1.48	36.8	0.63	0.993	80.1	3.14	0.611	3.9E-4	4.74	0.388	0.927	1.08	1.74	12.5	8.15	0.189	4.92E-4	9.52	0.088	0.559	8.69	0.107
1b - s	1.62	25.6	1.54	0.996	1130	9.95	0.722	1.81E-4	3.58	0.534	0.733	1.07	2.304	159	4.5	0.404	3.72E-5	1.21	0.441	0.772	0.59	0.673
1b - o	1.12	25.2	1.55	0.993	298	4.49	0.779	1.35E-4	1.49	0.472	0.7	0.98	1.258	47.4	4.93	0.189	1.17E-4	1.67	0.227	0.699	2.75	0.27
1c - s	1.51	23.5	1.24	0.96	221	4.36	0.822	4.88E-4	2.25	0.605	0.949	0.4	3.409	14.1	2.84	0.22	0.00197	2.73	0.131	0.447	2.34	0.124
1c - o	2.53	23.5	0.98	0.965	57.6	17.79	0.629	5.64E-4	2.68	0.42	0.968	0.84	2.031	9.4	7.25	0.193	0.0018	7.25	0.096	0.462	4.22	0.104
1d - s	1.44	22.3	1.2	0.96	315	4.16	0.858	3.8E-4	2.03	0.661	0.96	0.39	3.783	13.6	2.94	0.241	0.0013	2.19	0.136	0.479	2.5	0.139
1d - o	2.35	21.9	0.92	0.962	78.5	14.88	0.708	4.37E-4	2.54	0.49	0.966	0.75	2.339	8.88	6.08	0.202	0.00137	8.01	0.098	0.479	4.62	0.118
2a - s	1.28	28	1.05	0.936	157	3.87	0.737	9.16E-4	2.38	0.554	0.97	0.39	3.417	22.7	7.24	0.093	0.0208	2.07	0.146	0.232	5.13	0.131
2a - o	1.48	27.9	1.06	0.917	54.8	10.15	0.583	0.00112	2.24	0.383	0.956	0.57	2.073	10.2	4.21	0.138	0.0123	1.52	0.08	0.237	13.11	0.074
2b - s	1.94	25	1.33	0.969	214	4.88	0.785	4.85E-4	1.97	0.585	0.964	0.35	3.342	30.1	10.91	0.086	0.967	4.37	0.184	0.351	3.1	0.217
2b - o	3.59	25.2	0.34	0.959	75.4	25.02	0.659	5.71E-4	4.52	0.46	0.967	1.29	2.326	13.5	15.82	0.113	0.0109	11.64	0.112	0.32	18.44	0.111
2c – s	*4.55*	*36.6*	*0.82*	*0.99*	*7760*	*9.51*	*0.747*	*2.72E-5*	*6.88*	*0.573*	*0.808*	*1.39*	*2.851*	*1030*	*17.81*	*0.21*	*2.11E-5*	*8.52*	*0.322*	*0.858*	*2.84*	*0.978*
2c - o	*4.6*	*37.1*	*1.39*	*0.985*	*1110*	*23.99*	*0.985*	*7.46E-5*	*4.62*	*0.514*	*0.788*	*1.62*	*2.061*	*201*	*8.88*	*0.246*	*6.58E-5*	*3.39*	*0.356*	*0.719*	*4.86*	*0.562*
2d - s	3.28	34.9	1.97	0.961	78.1	0.061	28.04	3.26E-4	26.14	0.073	1.33	2.76	0.53	1970	0.789	7.09	1.35E-4	2.02	0.671	0.604	0.73	2.006
2d - o	4.08	35.9	0.35	0.966	104	30.44	0.554	1.94E-4	5.58	0.358	0.954	1.91	1.527	47.3	69.81	0.241	7.47E-4	6.92	0.231	0.498	8.3	0.268
3a - s	1.07	45.2	0.52	0.976	214	3.99	0.724	0.00113	2.25	0.555	0.964	0.34	3.545	21.2	9.53	0.065	0.0201	3.81	0.095	0.274	5.37	0.116
3a - o	2.06	50.9	3.59	0.971	66.6	9.2	0.512	0.00122	1.83	0.324	0.963	0.65	1.889	10.9	8.61	0.095	0.00876	28.66	0.051	0.306	16.91	0.05
3b - s	1.17	28.3	1.21	0.988	175	3.61	0.751	0.00102	2.07	0.567	0.84	0.32	3.668	24.9	7.8	0.094	0.00971	1.08	0.158	0.408	1.69	0.269
3b - o	1.53	27.2	1.44	0.987	49.9	11.65	0.564	0.00129	2.65	0.376	0.976	0.48	2.084	11.2	62.17	0.106	0.0121	9.35	0.092	0.391	6.59	0.138
3c - s	1.1	24.8	1.1	0.981	106	0.668	4.41	0.00106	1	0.478	0.972	0.36	2.822	27.3	0.151	4.36	0.00578	2.2	0.194	0.422	2	0.316
3c - o	2.11	23.8	0.87	0.983	29.8	0.457	19.34	0.00141	3.54	0.284	0.965	1.06	1.491	11.5	0.157	56.22	0.00755	9.4	0.108	0.415	7.93	0.153
3d - s	*4.29*	*31.5*	*2.17*	*0.855*	*6310*	*17.99*	*0.517*	*1.11E-4*	*3.9*	*0.61*	*0.694*	*3.95*	*3.013*	*463*	*7.17*	*0.148*	*2.92E-4*	*3.63*	*0.417*	*0.472*	*0.84*	*0.464*
3d - o	*88.1*	*92.4*	*26.34*	*1.086*	*902*	*67.81*	*0.858*	*5.96E-5*	*57.05*	*0.578*	*0.792*	*45.04*	*2.059*	*27.9*	*76.21*	*0.54*	*3.79E-10*	*65.23*	*0.631*	*1.6*	*13.46*	*3.058*
4a - s	1.01	51.5	0.6	0.975	60.9	0.455	3.88	0.0014	2.1	0.266	0.902	0.52	1.411	19.9	0.129	13.65	0.00572	6.45	0.087	0.354	6.73	0.111
4a - o	1.12	55.2	0.64	0.981	28	0.294	12.96	0.00149	5.08	0.145	0.873	1.35	0.665	10.7	0.122	4.34	0.00153	14.57	0.051	0.456	8.82	0.055
4b - s	1.95	23.3	1.85	0.927	70.9	4.17	0.595	0.00145	2.2	0.384	0.921	0.39	2.145	24.5	5.53	0.208	0.00624	5.36	0.187	0.321	5.43	0.203
4b - o	2.34	24.4	1.16	0.974	27.4	17.36	0.441	0.00161	7.56	0.23	0.834	2.25	0.96	9.07	7.41	0.229	2.93E-4	16.49	0.099	0.606	1.95	0.152
4c - s	*2.3*	*1460*	*0.94*	*1*	--	--	--	--	--	--	--	--	--	--	--	--	--	--	--	--	--	--
4c - o	*4.02*	*1040*	*5.18*	*1*	--	--	--	--	--	--	--	--	--	--	--	--	--	--	--	--	--	--
4d - s	2.39	27.2	1.56	0.926	129	0.658	5.34	0.0012	3.48	0.451	0.917	0.62	2.649	38.6	0.157	10.78	0.00816	5.07	0.22	0.291	6.88	0.245
4d - o	2.3	27.8	1.35	0.948	40.4	0.495	13.49	0.00155	6.43	0.278	0.871	1.6	1.321	11.6	0.222	6.97	0.00133	18.09	0.098	0.441	5.01	0.124
5a - s	2.02	28.2	1.33	0.945	91.5	4.42	0.618	0.00125	3.42	0.393	0.871	0.77	2.039	25.6	9.24	0.168	0.00625	5.98	0.167	0.33	7.27	0.185
5a - o	2.29	28.9	1.08	0.974	34.1	16.27	0.463	0.00142	4.25	0.245	0.835	1.86	1.031	9.07	8.16	0.197	4.28E-4	18.21	0.084	0.568	2.75	0.122
5b - s	0.821	80	0.57	0.99	71.7	0.415	3.7	0.00145	1.3	0.251	0.951	0.31	1.478	19.1	0.091	16.92	0.00812	8.12	0.058	0.363	4.7	0.091
5b - o	0.955	78.9	0.41	0.982	32.9	0.263	9.98	0.00157	3.67	0.138	0.922	1.09	0.711	12.3	0.089	29.41	0.00574	7.22	0.039	0.342	18.73	0.04
5d - s	*2.23*	*850*	*0.46*	*1*																		
5d - o	*73.17*	*81800*	*10.73*	*1*																		

s = short circuit, o = open circuit, Sig = significance.

3.3 Determination of hole collection time (τ_c) with IMPS

The controlled intensity modulated photovoltage spectroscopy (CIMPS) measurements were carried out using a Zahner CIMPS photoelectrochemical workstation (Zahner-Elektrik) controlled by CIMPS and Thales Z software packages (Zahner-Elektrik). The photocathodes were backlit with a white LED source (Zahner-Elektrik, TL04/LSW-2, see Figure SI–11 for spectral output). The cell was measured under potentiostatic conditions at 0 V. The measurements were carried out in a light exclusion box (Zahner-Elektrik). A dc light intensity of 100 mW·cm^{-2} was applied with an ac perturbation of 10 mW·cm^{-2}. The frequencies were scanned from 100 Hz to 300 mHz, with 10 steps·dec^{-1} above 66 Hz, and 5 steps·dec^{-1} below 66 Hz. At frequencies < 66 Hz, 4 measurement points were averaged at each measurement frequency; at the higher frequencies, 20 points were averaged at each frequency.

The obtained data was imported in the Zahner Analysis software, and the hole collection time (τ_c) was directly calculated from the Nyquist plot of the IMPS response via Equation SI–7.[30–32]

$$\tau_c = \frac{1}{\omega_{min,IMPS}} = \frac{1}{2\pi f_{min,IMPS}} \qquad (SI-7)$$

where $f_{min,IMPS}$ is the frequency corresponding to the minimum of the semicircle in the Nyquist plot, as shown in Figure SI–17.

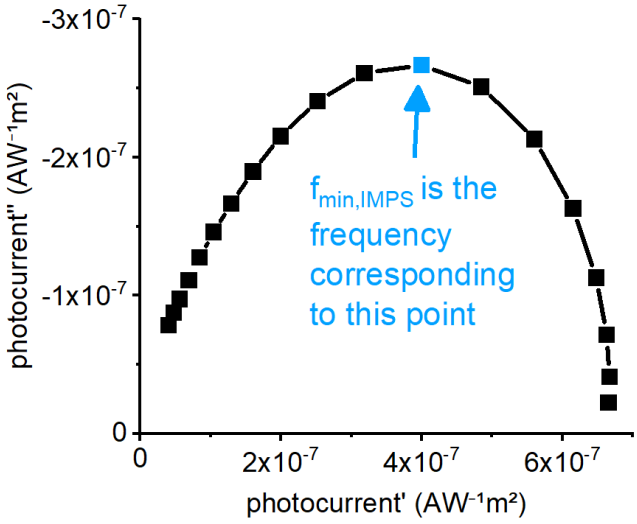

Figure SI–17. How $f_{min,IMVS}$ was retrieved from the –Nyquist plot of the IMPS data.

The assumptions and limitations that hold for IMVS (*vide supra*) also hold for deriving time constants from IMPS data. The hole collection times for the different solar cells are given in Table SI–10. The averages of τ_c in the main text (Figure 3, right panel) and Figure SI–18 were determined by calculating the mean of the values in Table SI–10. The error analysis was carried out by calculating the root-mean square between the sample mean and the observed values, *i.e.*, the sample standard deviation, using the *stddev* function in Origin (version 2018). The experimental error bars represent one standard deviation.

Table SI–10. Hole collection times under 100 mW·cm^{-2} illumination and short–circuit conditions (0 V).

Solar cell	τ_c (s)	Solar cell	τ_c (s)
1a	0.011	3b	0.028
1b	0.005	3c	0.020
1c	0.011	4a	0.028
1d	0.011	4b	0.028
2a	0.028	4d	0.028
2b	0.011	5a	0.020
2d	0.006	5b	0.041
3a	0.041		

The hole collection time shows a linear dependency on the number of NiO layers, as depicted in Figure SI–18. The data was fitted to a linear function using Origin software (version 2018).

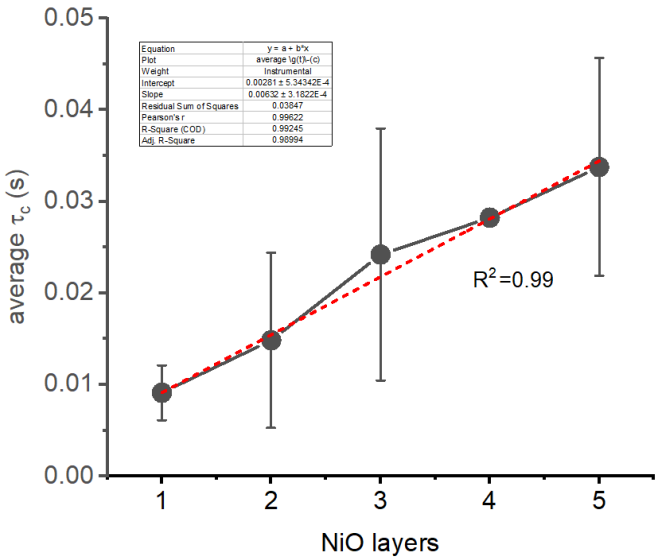

Figure SI–18. Correlation between the number of NiO layers and the average hole collection time.

3.4 Comments on the NiO thickness and how it relates to the solar cell efficiency

The reported (ideal) thickness of the doctor-bladed NiO electrode in literature tends to vary between 700 nm to 2.5 μm (Table SI–11), where the most common values are 1.1–1.2 μm (three references) and 1.5 μm (three references).

Table SI–11. Reported values on the thickness of the doctor-bladed NiO electrodes.

Reported thickness (μm)	doctor-blade cycles	reference
0.70 ± 0.05	1	35
1.1 ± 0.02	3	36
1.1–1.2	2	3
1.2	2	37
*ca.*1.3	3	38
1.5 ± 0.22	3	39
1.5	3	40
1.5	multiple	31
ca. 1.6	2	21
1.8–1.9 2.0–2.2 2.0–2.5	multiple	41
ca. 2.0	multiple	42
2.0	multiple	43

We have compared the performance of our NiO electrodes with a similar thickness, as described in Table SI–12, to investigate if a reproduced thickness results in reproducible performance in the *p*-DSSC. Four classes of NiO thickness were compared: 0.66–0.70, 0.93–0.96, 1.19–1.20 and 1.83–1.85 μm in the benchmark P1 DSSC, where we compared the overall solar cell efficiency (η), the short-circuit current (J_{SC}), the hole collection time (τ_c), the hole recombination time (τ_n) and the charge collection efficiency (η_{cc}).

Table SI–12. Comparing the properties and performance of NiO electrodes with similar thickness in the benchmark P1 DSSC.

	solar cells		
	1b	*1d*	*2b*
thickness (µm)	**0.70**	**0.66**	**0.68**
η (%)	0.032	0.083	0.114
J_{SC} (mA·cm^{-2})	–1.019	–2.385	–3.196
τ_c	0.005	0.011	0.011
τ_n	0.115	0.110	0.095
η_{cc}	0.960	0.903	0.889
	2d	*3a*	
thickness (µm)	**0.96**	**0.93**	
η (%)	0.075	0.041	
J_{SC} (mA·cm^{-2})	–1.489	–1.533	
τ_c	0.006	0.041	
τ_n	0.063	0.229	
η_{cc}	0.905	0.823	
	3b	*4d*	
thickness (µm)	**1.20**	**1.19**	
η (%)	0.087	0.106	
J_{SC} (mA·cm^{-2})	–3.037	–3.742	
τ_c	0.028	0.028	
τ_n	0.129	0.131	
η_{cc}	0.780	0.784	
	4a	*4b*	
thickness (µm)	**1.85**	**1.88**	
η (%)	0.098	0.19	
J_{SC} (mA·cm^{-2})	–3.535	–6.154	
τ_c	0.028	0.028	
τ_n	0.065	0.086	
η_{cc}	0.567	0.665	

These results show that the solar cell performance at identical measured NiO thickness still deviates very significantly, and thus that the film thickness is also not a very reliable metric to predict the solar cell performance. Nevertheless, similar trends in the collection time, recombination time and charge collection efficiency could be obtained with increasing NiO thickness as those observed with an increasing number of NiO layers:

- We found no correlation between the NiO thickness and the hole recombination time (τ_n; Figure SI–19, left).
- No significant linear correlation was found between the hole collection time (τ_c, Figure SI–19, middle).
- A stronger linear correlation was found between the charge collection efficiency (η_{cc}) and NiO thickness (Figure SI–19, right).

The correlations between τ_c and η_{cc} to the NiO thickness are more spread out (lower R^2 values) compared to the correlations to the number of NiO layers (see Figures 3 and SI–17). A reason for this could be the additional error that is introduced in the data during the thickness measurements, and the fact that the data versus the number of NiO layers is averaged.

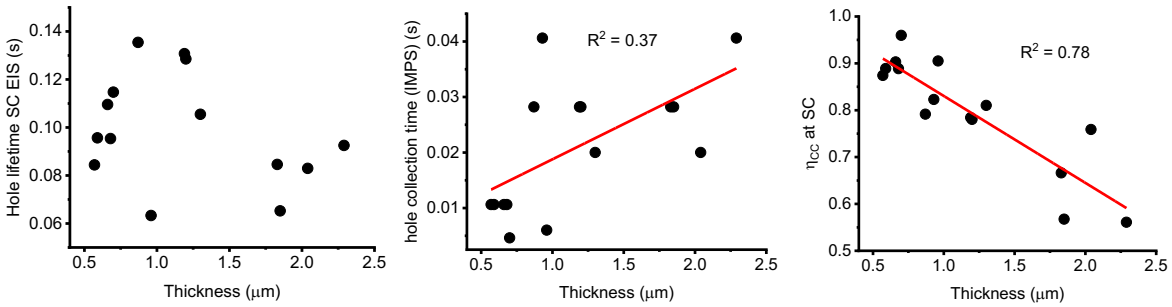

Figure SI–19. Correlation between NiO thickness and the measured hole lifetime (left), measured hole collection time (middle) and calculated charge collection efficiency (right). The data was fitted to a linear function using Origin software (version 2018).

References and notes

1 M. Bonomo, D. Di Girolamo, M. Piccinni, D. P. Dowling and D. Dini, *Nanomaterials*, 2020, **10**, doi:10.3390/nano10010167.

2 S. Sumikura, S. Mori, S. Shimizu, H. Usami and E. Suzuki, *J. Photochem. Photobiol. A*, 2008, **199**, 1.

3 L. Li, E. A. Gibson, P. Qin, G. Boschloo, M. Gorlov, A. Hagfeldt and L. Sun, *Adv. Mater.*, 2010, **22**, 1759.

4 Once the tape touches the glass, that piece of FTO glass is contaminated, and a good connection between that piece of FTO and NiO cannot be guaranteed anymore. Care was taken to properly place the piece of tape in one attempt.

5 If excess solution is not swiped off the plate, it tends to flow back onto the spot and generates an inhomogeneous NiO electrode once sintered.

6 Doctor-blading can be carried out in multiple ways, but usually involves masking the substrate with tape, and spreading a solution or paste with a certain object. We have tried different ways of masking the substrate with tape, for instance by taping off the sides, or by making a square well using four small pieces of tape, but the best results were obtained using a circular well. We have also tried smearing out the precursor solution with a sharper object than the glass rod, such as a glass plate, but this led to slightly poorer performing solar cells.

7 The tape tends to stick strongly to the electrodeposited NiO, which can cause the tape to rip and tear, if not pulled off correctly. The most successful technique has been by folding the tape over 180°, and then start pulling on the tape gently, rather than applying a lot of force or pulling at a 90° angle.

8 The reproducibility issues regarding the position and occupancy within the furnace have not completely been resolved yet. We have observed NiO coming out of the oven in various forms: transparent grey; transparent dark brown-blackish, or a mix thereof. We recently found that the brown-black form can be transformed into the transparent grey form if sintered for a longer period. This might indicate that the brown-black form is a form in which the sintering process is not completed yet. We find the brown-black form especially when the furnace is relatively full, or we find it in the plates that are in the centre of the oven or close to the oven door, relatively far away from the heating source. We speculate that improper circulation of heat and/or oxygen can lead to increased deviations in the NiO plates, since the sintering of some plates might have proceeded to a different level than others. Gibson et al. also reported that sintering from $Ni(OH)_2$ to NiO is accompanied by a colour change from green to black to light grey,[33] hinting towards incomplete sintering in case of the black NiO spots.

9 If the NiO spots were not grey (checked by opening the furnace door), the furnace door was closed again, and the temperature was kept at 450 °C. Every five minutes, the colour of the NiO was checked. In case of a full oven (> 20 samples), it could sometimes take up to an additional 20 minutes before all the spots had the same colour. Even the spots close to the heating element would still be black-brown after 30 minutes.

10 The plates must cool down as soon as possible after the temperature programme has finished. Every minute they stay in the oven longer, the sintering process continues, effecting the properties of the formed NiO particles. Care must be taken when taking out the plates at this temperature, by wearing a lab coat, heat-protective gloves and use long stainless-steel tweezers. If the glass cracks upon touching it with the tweezers, this is caused by temperature difference between the tweezers and the FTO. It can be prevented by heating the tip of the tweezers on the 180 °C plate for a couple of seconds.

11 Sun et al.[3] found that stepwise doctor-blading and sintering of the $NiCl_2$ precursor solution resulted in more efficient solar cells, compared to when multiple layers of tape were stacked, and a thicker precursor solution layer was doctor-bladed.

12 C. Y. Lin, J. Y. Lin, C. C. Wan and T. C. Wei, *Electrochim. Acta*, 2011, **56**, 1941.

13 D. F. Bruggeman, T. M. A. Bakker, S. Mathew and J. N. H. Reek, *Chem. Eur. J.*, 2021, **27**, 218.

14 T. Bouwens, T. M. A. Bakker, K. Zhu, J. Hasenack, M. Dieperink, A. M. Brouwer, A. Huijser, S. Mathew and J. N. H. Reek, *Nat. Chem.*, 2023, **15**, 213.

15 In our experience, rough edges of the thermoplastic frame can result into air bubbles when filling the cell with electrolyte. Also, melting the polymer without folding was more difficult if the edges were rough. Finally, rough edges may lead to some of the FTO still being exposed. It is hard to quantify this, but smooth edges generally led to more reproducible results.

16 Although hard to quantify, applying a vacuum for longer periods of time influences the solar cell performance. The time between applying the electrolyte drop on the hole and sealing of the cell should thus be as short as possible.

17 S. Lyu, J. Massin, M. Pavone, A. B. Muñoz-García, C. Labrugère, T. Toupance, M. Chavarot-Kerlidou, V. Artero and C. Olivier, *ACS Appl. Energy Mater.*, 2019, **2**, 4971.

18 D. Ameline, S. Diring, Y. Farre, Y. Pellegrin, G. Naponiello, E. Blart, B. Charrier, D. Dini, D. Jacquemin and F. Odobel, *RSC Adv.*, 2015, **5**, 85530.

19 P. Qin, H. Zhu, T. Edvinsson, G. Boschloo, A. Hagfeldt and L. Sun, *J. Am. Chem. Soc.*, 2008, **130**, 8570.

20 C. J. Wood, G. H. Summers, C. A. Clark, N. Kaeffer, M. Braeutigam, L. Roberta Carbone, L. D'Amario,K. Fan, Y. Farré, S. Narbey, F. Oswald, L. A. Stevens, C. D. J. Parmenter, M. W. Fay, A. La Torre, C. E. Snape, B. Dietzek, D. Dini, L. Hammarström, Y. Pellegrin, F. Odobel, L. Sun, V. Artero and E. A. Gibson, *Phys. Chem. Chem. Phys.*, 2016, **18**, 10727.

21 L. Zhu, H. Yang, C. Zhong and C. M. Li, *Chem. Asian J.*, 2012, **7**, 2791.

22 J. Cui, J. Lu, X. Xu, K. Cao, Z. Wang, G. Alemu, H. Yuang, Y. Shen, J. Xu, Y. Cheng and M. Wang, *J. Phys. Chem. C*, 2014, **118**, 16433.

23 M. Bonomo, D. Gatti, C. Barolo and D. Dini, *Coatings*, 2018, **8**, 232.

24 C.-H. Chang, Y.-C. Chen, C.-Y. Hsu, H.-H. Chou and J. T. Lin, *Org. Lett.*, 2012, **14**, 4726.

25 J. van de Lagemaat, N. G. Park and A. J. Frank, *J. Phys. Chem. B*, 2000, **104**, 2044.

26 J. Bisquert, F. Fabregat-Santiago, I. Mora-Seró, G. Garcia-Belmonte and S. Giménez, *J. Phys. Chem. C*, 2009, **113**, 17278.

27 D. Klotz, D. S. Ellis, H. Dotan and A. Rothschild, *Phys. Chem. Chem. Phys.*, 2016, **18**, 23438.

28 L. Dloczik, O. Ileperuma, I. Lauermann, L. M. Peter, E. A. Ponomarev, G. Redmond, N. J. Shaw and I. Uhlendorf, *J. Phys. Chem. B*, 1997, **101**, 10281.

29 X. L. Zhang, Z. Zhang, F. Huang, P. Bäuerle, U. Bach and Y. B. Cheng, *J. Mater. Chem.*, 2012, **22**, 7005.

30 P. A. DeSario, J. J. Pietron, D. H. Taffa, R. Compton, S. Schünemann, R. Marschall, T. H. Brintlinger, R. M. Stroud, M. Wark, J. C. Owrutsky and D. R. Rolison, *J. Phys. Chem. C*, 2015, **119**, 17529.

31 Z. Huang, G. Natu, Z. Ji, M. He, M. Yu and Y. Wu, *J. Phys. Chem. C*, 2012, **116**, 26239.

32 M. Raïssi, Y. Pellegrin, F. X. Lefevre, M. Boujtita, D. Rousseau, T. Berthelot and F. Odobel, *Sol. Energy*, 2020, **199**, 92.

33 J. Halme, *Phys. Chem. Chem. Phys.*, 2011, **13**, 12435.

34 D. Dini, Y. Halpin, J. G. Vos and E. A. Gibson, *Coord. Chem. Rev.*, 2015, **304–305**, 179.

35 L. D'Amario, G. Boschloo, A. Hagfeldt and L. Hammarström, *J. Phys. Chem. C*, 2014, **118**, 19556.

36 Q. Liu, L. Wei, S. Yuan, X. Ren, Y. Zhao, Z. Wang, M. Zhang, L. Shi and D. Li, *J. Mater. Sci.*, 2015, **50**, 6668.

37 P. Qin, J. Wiberg, E. A. Gibson, M. Linder, L. Li, T. Brinck, A. Hagfeldt, B. Albinsson and L. Sun, *J. Phys. Chem. C*, 2010, **114**, 4738.

38 L. Tian, T. Törndahl, J. Lin, P. B. Pati, Z. Zhang, T. Kubart, Y. Hao, J. Sun, G. Boschloo and H. Tian, *J. Phys. Chem. C*, 2019, **123**, 26151.

39 L. Wei, L. Jiang, S. Yuan, X. Ren, Y. Zhao, Z. Wang, M. Zhang, L. Shi and D. Li, *Electrochim. Acta*, 2016, **188**, 309.

40 M. Zannotti, E. Benazzi, L. A. Stevens, M. Minicucci, L. Bruce, C. E. Snape, E. A. Gibson and R. Giovannetti, *ACS Appl. Energy Mater.*, 2019, **2**, 7345.

41 K. A. Click, D. R. Beauchamp, B. R. Garrett, Z. Huang, C. M. Hadad and Y. Wu, *Phys. Chem. Chem. Phys.*, 2014, **16**, 26103.

42 E. A. Gibson, A. L. Smeigh, L. Le Pleux, L. Hammarström, F. Odobel, G. Boschloo and A. Hagfeldt, *J. Phys. Chem. C*, 2011, **115**, 9772.

43 E. A. Gibson, L. Le Pleux, J. Fortage, Y. Pellegrin, E. Blart, F. Odobel, A. Hagfeldt and G. Boschloo, *Langmuir*, 2012, **28**, 6485.